

Spin-echo spectroscopy with ultracold neutrons

S. Afach,^{1,2,3} N.J. Ayres,⁴ G. Ban,⁵ G. Bison,¹ K. Bodek,⁶ Z. Chowdhuri,¹ M. Daum,¹
M. Fertl,^{1,2,*} B. Franke,^{1,2,†} W.C. Griffith,⁴ Z.D. Grujić,⁷ P.G. Harris,⁴ W. Heil,⁸
V. Hélaine,^{1,5,‡} M. Kasprzak,⁷ Y. Kermaidic,⁹ K. Kirch,^{1,2} P. Knowles,^{7,§} H.-C. Koch,^{7,8}
S. Komposch,^{1,2} A. Kozela,¹⁰ J. Krempel,² B. Lauss,¹ T. Lefort,⁵ Y. Lemièrre,⁵ A. Mtchedlishvili,¹
M. Musgrave,⁴ O. Naviliat-Cunic,^{5,¶} J.M. Pendlebury,⁴ F.M. Piegsa,² G. Pignol,⁹
C. Plonka-Spehr,¹¹ P.N. Prashanth,¹² G. Quémener,⁵ M. Rawlik,² D. Rebreyend,⁹ D. Ries,^{1,2}
S. Roccia,¹³ D. Rozpedzik,⁶ P. Schmidt-Wellenburg,^{1,**} N. Severijns,¹² J.A. Thorne,⁴
A. Weis,⁷ E. Wursten,¹² G. Wyszynski,⁶ J. Zejma,⁶ J. Zenner,^{1,2,11} and G. Zsigmond¹

¹Paul Scherrer Institut, CH-5232 Villigen PSI, Switzerland

²ETH Zürich, Institute for Particle Physics, CH-8093 Zürich, Switzerland

³Hans Berger Department of Neurology, Jena University Hospital, D-07747 Jena, Germany

⁴Department of Physics and Astronomy, University of Sussex, Falmer, Brighton BN1 9QH, UK

⁵LPC Caen, ENSICAEN, Université de Caen, CNRS/IN2P3, Caen, France

⁶Marian Smoluchowski Institute of Physics, Jagiellonian University, 30-059 Cracow, Poland

⁷Physics Department, University of Fribourg, CH-1700 Fribourg, Switzerland

⁸Institut für Physik, Johannes-Gutenberg-Universität, D-55128 Mainz, Germany

⁹LPSC, Université Grenoble Alpes, CNRS/IN2P3, Grenoble, France

¹⁰Henryk Niedwodniczanski Institute for Nuclear Physics, Cracow, Poland

¹¹Institut für Kernchemie, Johannes-Gutenberg-Universität, Mainz, Germany

¹²Instituut voor Kern- en Stralingsfysica, Katholieke Universiteit Leuven, B-3001 Leuven, Belgium

¹³CSNSM, Université Paris Sud, CNRS/IN2P3, Orsay, France

We describe a spin-echo method for ultracold neutrons (UCNs) confined in a precession chamber and exposed to a $|B_0| = 1 \mu\text{T}$ magnetic field. We demonstrate a gravity-dependent spin dephasing by applying small vertical magnetic field gradients. The method gives access to the energy spectrum of stored UCNs, which can be crucial for the assessment of systematic effects in precision experiments such as searches for an electric dipole moment of the neutron.

Keywords: ultracold neutrons, energy spectrum, spin precession, spin-echo

Spin-echo resonances, first observed by Hahn in 1950 [1], have proven to be a very powerful tool in nuclear magnetic resonance (NMR) experiments for identifying different sources of depolarization in spin-polarized samples. In particular, the $\pi/2 - \pi$ pulse sequence proposed by Carr and Purcell [2] is widely applied to distinguish the intrinsic spin-lattice or spin-spin coherence time T_2 from the global coherence time T_2^* dominated by dephasing of precessing spins due to spatially varying magnetic fields. Another established application of the spin-echo technique is in neutron scattering [3] where it is used to resolve correlation times below $1 \mu\text{s}$. Essentially the spin-echo technique can be applied in solid and soft matter samples where the intrinsic component is long compared to dephasing, which can even be the case for $T_2 \ll 1\text{ s}$. Two similar components of depolarization [4] exist in experiments using UCNs [5–11] where coherence times T_2^* of several hundred seconds have been achieved.

The defining characteristic of UCNs is that they are reflected from appropriate material surfaces at all angles of incidence, even at room temperature, conserving kinetic energy as they do so. They can therefore be confined for observation times that are commensurate with neutron β -decay: inelastic scattering with phonons from the storage-vessel walls contributes $\Gamma \approx 10^{-3}\text{ s}^{-1}$ to their loss rate. Ultracold neutrons have kinetic energies E_{kin} of the same order of magnitude as their gravitational potential energy E_{pot} above the lower confining surface. For any given UCN $E = E_{\text{kin}} + E_{\text{pot}}$ is constant during storage, although for the ensemble the average energy decreases over time because faster neutrons have a higher loss rate. For neutrons $mg \approx 1.03\text{ neV/cm}$, so, e.g., UCN with kinetic energy of 200 neV can rise about 200 cm in the gravitational field. Therefore, it is convenient (and common) to refer to the energy ϵ of UCN in terms of the maximum height (in cm) attainable within Earth's gravitational field, and we do so here during our analysis, although we revert to E (in neV) for our final results.

Two channels of field-induced depolarization of UCNs exist: the well known intrinsic depolarization due to inhomogeneous magnetic fields [12–17], and an energy-dependent relative dephasing for different energies in a vertical magnetic field gradient. This latter interplay between gravitationally defined spatial distributions of the neutrons and a vertical magnetic-field gradient $\partial B_z/\partial z$ has only recently been studied theoretically [4, 18], and is the subject of this investigation using a new form of spin-echo spectroscopy. Prior to this, the spin-echo resonance method was used in a study of Berry's phase with UCNs to cancel any dynamic phase shift [19] with a coherence time of approximately 850 ms .

We have measured UCN spin-echo signals using an apparatus dedicated to the neutron electric dipole moment (nEDM) experiment [20] with a vertical magnetic field of $B_0 = -1 \mu\text{T}$ and depolarization times of

more than 450 s. These measurements, together with knowledge of the magnetic field gradients, were used to determine the energy spectrum of the UCN after storage.

The equilibrium density distribution of UCNs as a function of height h above the lower confinement surface in a bottle with diffusely scattering walls is $\rho(h) = \rho(0) \cdot \sqrt{1 - h/\epsilon}$ [21]. This leads to a center-of-mass offset of $H/2 - \langle h(\epsilon) \rangle$ relative to the center plane of a cylindrical precession chamber of height H , where

$$\langle h(\epsilon) \rangle = \begin{cases} \frac{2}{5}\epsilon & \text{for } \epsilon < H \\ \frac{\epsilon(\frac{2}{5} - \eta + \frac{3}{5}\eta^{5/3})}{1 - \eta} & \text{for } \epsilon \geq H \end{cases} \quad (1)$$

is the time-averaged height of a neutron [4] with $\eta = (1 - H/\epsilon)^{3/2}$.

In the presence of a vertical magnetic-field gradient, neutrons with an energy ϵ will precess with an average Larmor frequency of

$$\omega(\epsilon) = \gamma_n \left(\pm \langle B_0 \rangle - \frac{\partial B_z}{\partial z} (H/2 - \langle h(\epsilon) \rangle) \right), \quad (2)$$

where $\pm \langle B_0 \rangle$ is the volume-averaged magnetic field magnitude in the precession chamber for B_0 up (+) or down (-), and $\gamma_n = -2\pi \cdot 29.1646943(69)$ MHz/T [22]. This induces an energy-dependent relative phase $\Phi(\epsilon) = \omega(\epsilon) \cdot T$, where T is the free spin-precession (FSP) time. It leads to a relative dephasing which, when averaged over the energy spectrum, can be interpreted as a gravitationally enhanced depolarization. This relative dephasing can be studied by applying a $\pi/2 - \pi - \pi/2$ spin-echo sequence, varying the time t_1 at which the π -pulse of duration t_π is applied while keeping constant the total duration $T + t_\pi$ between the end of the first and start of the second $\pi/2$ pulses. The second $\pi/2$ pulse, at the end of the sequence, is required to transfer information about the spin-precession phase onto the measurable longitudinal spin component. For convenience, we analyze the system in a rotating frame precessing with $\omega_0 = \gamma_n \cdot \langle B_0 \rangle$ and $B_0 > 0$ inside the storage volume, and we only consider a linear gradient $\partial B_z / \partial z$ along the primary B_0 field axis z . Therefore, in the rotating frame, the spins of UCNs with energy E precess with average frequency (to first order in $\partial B_z / \partial z$)

$$\omega_r(\epsilon) = -\gamma_n \frac{\partial B_z}{\partial z} \cdot (H/2 - \langle h(\epsilon) \rangle). \quad (3)$$

Figure 1 illustrates the evolution of the spins in the rotating frame. The resonance condition under which the spins of all different energies refocus is established when $T = 2t_1$. At this time we measure the highest polarization, which is essentially the polarization $\langle \alpha(T, \epsilon) \rangle_\epsilon$ without the gravitationally induced dephasing. If we change the start time t_1 of the π -pulse to values shorter than $T/2$, the resonance condition will have been met before we apply the second $\pi/2$ -pulse. As the spins of the different energy classes then proceed to fan out again, the final polarization decreases. Similarly, if the π -pulse is applied at times larger than $T/2$ the refocusing is not yet complete by the time the second $\pi/2$ -pulse is applied.

For a particular UCN energy ϵ and fixed T the observed polarization after the second $\pi/2$ -pulse can be written as

$$P(\epsilon, t_1) = \alpha(T, \epsilon) \cdot \cos[\omega_r(\epsilon) (T - 2t_1)]. \quad (4)$$

By integrating over the UCN energy spectrum $p(\epsilon)$ at the time of polarization analysis the observed polarization is then

$$P(t_1) = \int \alpha(T, \epsilon) \cdot \cos[\omega_r(\epsilon) (T - 2t_1)] p(\epsilon) d\epsilon, \quad (5)$$

where $p(\epsilon)$ is normalized to 1.

We have used the MCUCN package [23] with a detailed model of the nEDM experiment at PSI [20] and simulated the measurement with a $\pi/2 - \pi - \pi/2$ spin-flip sequence (tip - flip - tip) for a fully polarized initial population of UCNs. This simulation was carried out for two different UCN energy spectra $p(\epsilon)$, parametrized as in equation (7) below, each with three different constant vertical gradients of $\partial B_z / \partial z = 100, 200$, and 400 pT/cm for a free precession time of 92 s. The resulting simulated spin-echo resonances are shown in the

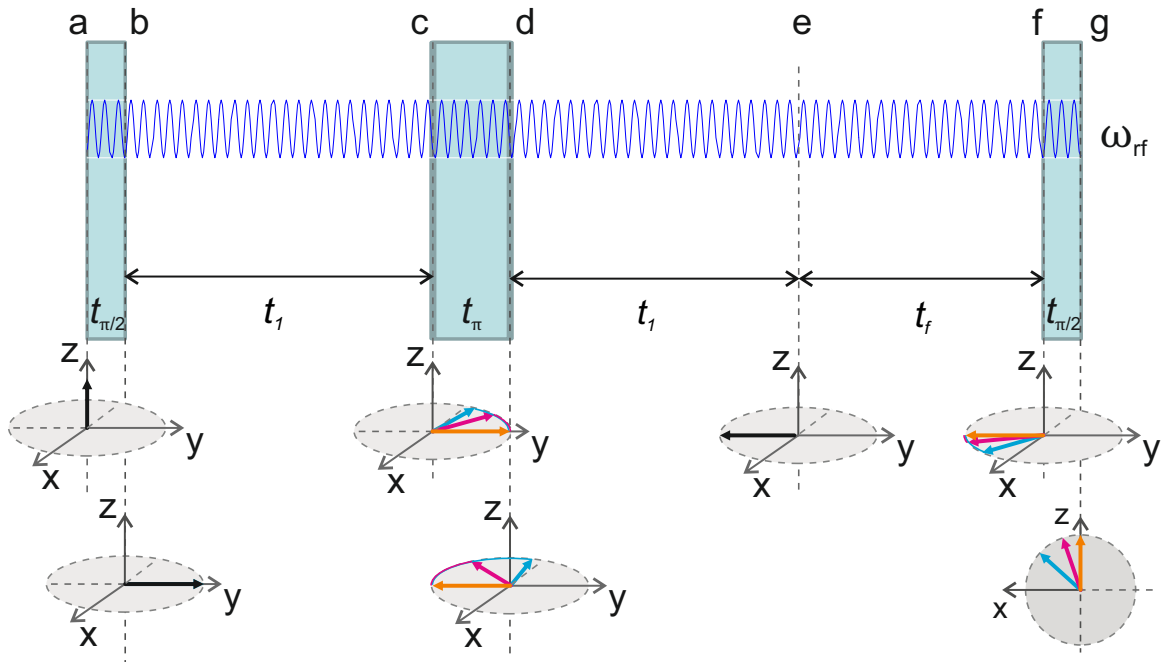


Figure 1: Illustration of a UCN spin-echo measurement of duration $T = 2t_1 + t_f$ in the frame rotating at frequency $\omega_{\text{rf}} = \omega_0$ for a negative gradient $\partial B_z / \partial z$: (a) a polarized ensemble of UCNs is loaded to the cell, (a-b) an initial $\pi/2$ -pulse tips all spins (black arrow) into the equatorial plane, (b-c) the UCN spins precess with $\omega_r(E)$ for t_1 and fan out. Low-energy UCNs (blue) see a larger (smaller) field for a negative (positive) gradient $\partial B_z / \partial z$ than higher-energy UCNs (magenta), whereas spins that precess at ω_0 (i.e. with no center-of-mass offset) are stationary and are oriented along y . A π -pulse (c-d) then flips the spins around the x -axis, after which (d-e) the UCNs continue to precess in the same direction, eventually refocusing at $2t_1$ (black arrow). As they continue to precess beyond this time they fan out again (e-f) until finally (f-g) a second $\pi/2$ pulse is applied. All pulses used for spin manipulation have the same field strength B_x applied along the same axis (x). A single oscillator is used, with the output being gated on only during the blue time windows; hence, all of the pulses are phase coherent with each other. All energy-dependent effects during the pulses cancel, since a full rotation about 2π is made and only dephasing during FSP has to be taken into account.

inserts of Fig. 2. For analysis, we performed least-squares fits of equation (5) to the simulated signals. In particular, we used $\alpha(T, \epsilon) = \alpha_0 \exp(-T \cdot \Gamma_2(\epsilon))$, with a transverse relaxation rate $\Gamma_2(\epsilon)$ of [12]

$$\Gamma_2(\epsilon) = a\gamma_n^2 \frac{\lambda(\epsilon)}{v(\epsilon)} \left[R^2 \left(\left| \frac{\partial B_z}{\partial x} \right|^2 + \left| \frac{\partial B_z}{\partial y} \right|^2 \right) + 2\mathcal{H}^2(\epsilon) \left| \frac{\partial B_z}{\partial z} \right|^2 \right], \quad (6)$$

where $\lambda(\epsilon)$, $v(\epsilon)$, and $\mathcal{H}(\epsilon) = \epsilon \forall \epsilon \leq H$ and $\mathcal{H}(\epsilon) = H \forall \epsilon > H$ are the energy-dependent mean free path, velocity, and effective height of the UCN as introduced in [21] for a cylindrical cell of height H and radius R ; a is a free fit parameter. Equation(6) matches the simulated intrinsic UCN depolarization of Ref. [4] as shown in Fig. 2 of [4]. We found it useful to model the UCN spectrum as

$$p(\epsilon) = \frac{A \cdot \epsilon^{1/2}}{1 + e^{(E_0 - \epsilon)/b^2}} \cdot \left(\frac{1}{1 + e^{(\epsilon - (E_0 + E_1))/c^2}} - \frac{1}{1 + e^{E_2 - E_0 - E_1/c^2}} \right), \quad (7)$$

where E_0 , b and $E_0 + E_1$, c are the points of inflection and slopes of the rising and falling energy edges respectively, while $E_0 + E_1 + E_2$ is the high-energy cut-off. A is chosen such that $\int_0^{E_0 + E_1 + E_2} p(\epsilon) d\epsilon = 1$. This energy spectrum is based on a very general distribution $n(\epsilon)d\epsilon \propto \epsilon^{1/2}d\epsilon$ from the low-energy tail of a Maxwell-Boltzmann distribution, allowing for low- and high-energy cut-offs. A simultaneous fit to the signals of all three gradients yielded a , b , c , E_0 , E_1 , and E_2 for each of the two spectra. For the numerical integration of equation (5) we used energy bins of equal height: $\Delta h(\epsilon) = 0.2$ mm, which is sufficiently small that any systematic error from the finite energy bins would be less than than the statistical resolution of each data point. Figure 2 compares spectra extracted from the fit to the input spectra of the simulation. We

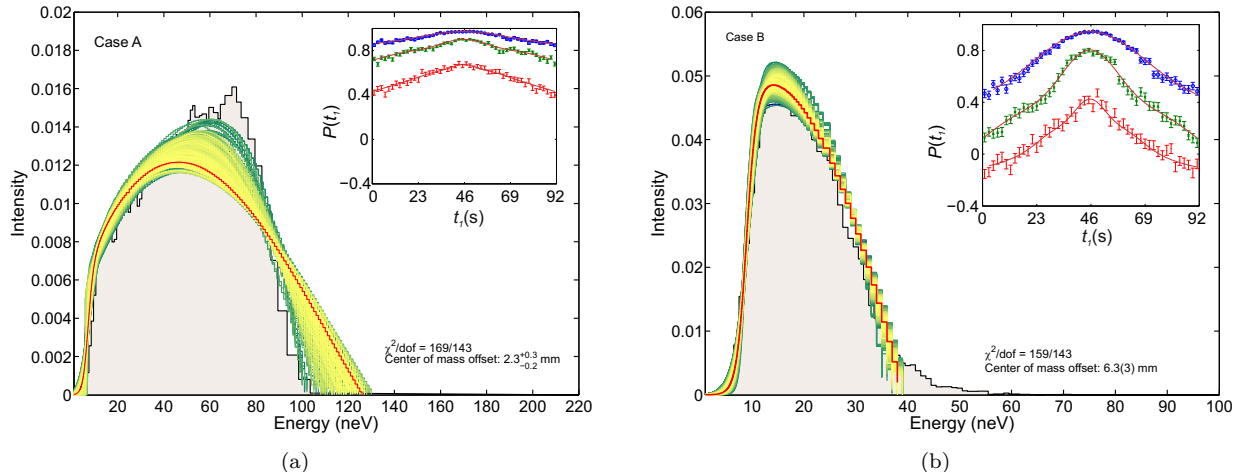


Figure 2: Simulated spin-echo signals and extracted spectra. The inserts show the simulated spin-echo signals using MCUCN[23]. On each plot three resonances are shown, using the grey input spectra with three different vertical field gradients: blue 100 pT/cm; green 200 pT/cm; and red 400 pT/cm. The points with their uncertainties come from the simulation. The red lines on the main plots are the best simultaneous fits to the simulated spectra. The colors (from bright yellow to dark green) represent the χ^2 value for each line; dark green corresponds to a 68.3% C.L while bright yellow lines have χ^2 values close to the minimum. The original input spectra are represented by the grey areas, which give center-of-mass offsets of 1.93 mm (Case A) and 6.46 mm (Case B).

note that the results become less reliable at higher energies; this is to be expected, since once the neutrons populate the bottle more or less uniformly it becomes increasingly difficult to discriminate between them.

We measured three spin-echo profiles (see Fig.3) using the apparatus described in Ref. [24], improved with an array of 16 cesium vapor magnetometers (CsM) [25] and a simultaneous spin-analyzing system [26]. The magnetic field measurement with the CsM array permitted us to calculate the magnetic-field gradients using a polynomial field decomposition up to second order, as described in Ref. [22]. Data were taken for a constant FSP duration of $T = 216$ s, with three different trim-coil current settings for $B_0 < 0$ (down), thereby applying vertical gradients of $\partial B_z / \partial z = -18, 10,$ and 38 pT/cm. The uncertainties of the gradient measurements are dominated by systematics due to individual sensor offsets, and amount to 12-14 pT/cm (see [22, 31] for a determination of these gradient errors). However, under our conditions, such individual but constant offsets lead to a constant offset G_z of the true $\partial B_z / \partial z$ that can be determined to within 1-2 pT/cm. We will determine G_z in our treatment below.

The measured initial polarization $\alpha_0 = 0.861(2), 0.865(2), 0.861(2)$ was prepared by passing UCNs from the spallation-based UCN source at the Paul Scherrer Institute [27] through a 5 T solenoid magnet. After a filling time of 24 s, the UCN shutter in the ground electrode was closed. For each setting, one fixed radio frequency ω_{rf} was used. The mercury co-magnetometer measured the mean magnetic field B_0 via $\omega_{Hg} = \gamma_{Hg} \cdot \langle B_0 \rangle$ [28].

An initial 2 s long $\pi/2$ pulse tipped the neutron spins into the plane perpendicular to the main magnetic field B_0 . After a precession time t_1 the neutron spins were flipped by a π pulse (4 s long) coherent with the first pulse. After a second FSP period of duration $t_1 + t_f$ a second $\pi/2$ pulse, in phase with the two earlier pulses, was applied. The UCN shutter was then opened again, and the UCN were detected in a pair of spin-state specific detector channels. A measurement consisted of several cycles with t_1 increasing in steps of 9 s. Figure 3 shows the three measured spin-echo resonances. As for the simulated cases, equation (5) was fitted to the data, using the same fitting procedure. The frequency ω_r from equation (3) was corrected for the difference $\Delta\omega = \omega_{rf} - |\gamma_n|/\gamma_{Hg}\omega_{Hg}$ and was also extended by a term for the second-order gradient in z , which was available from the field measurement:

$$\omega_r(\epsilon) = \gamma_n \left(- \left(\frac{\partial B_z}{\partial z} + G_z \right) \cdot (H/2 - \langle h(\epsilon) \rangle) + \frac{\partial^2 B_z}{\partial z^2} \cdot (\langle h^2 \rangle - \langle (H/2 - h(\epsilon))^2 \rangle) \right) - \Delta\omega, \quad (8)$$

where $\langle h^2 \rangle = \int_{-6}^{+6} z^2 / H dz = 12 \text{ cm}^2$ is the spectrum-independent quadratic expectation value. We used the extracted gradient values ($\partial B_z / \partial z, \partial^2 B_z / \partial z^2$) and the initial polarization α_0 as direct measured inputs. The fit parameter G_z was included to accommodate the above-mentioned common gradient offset.

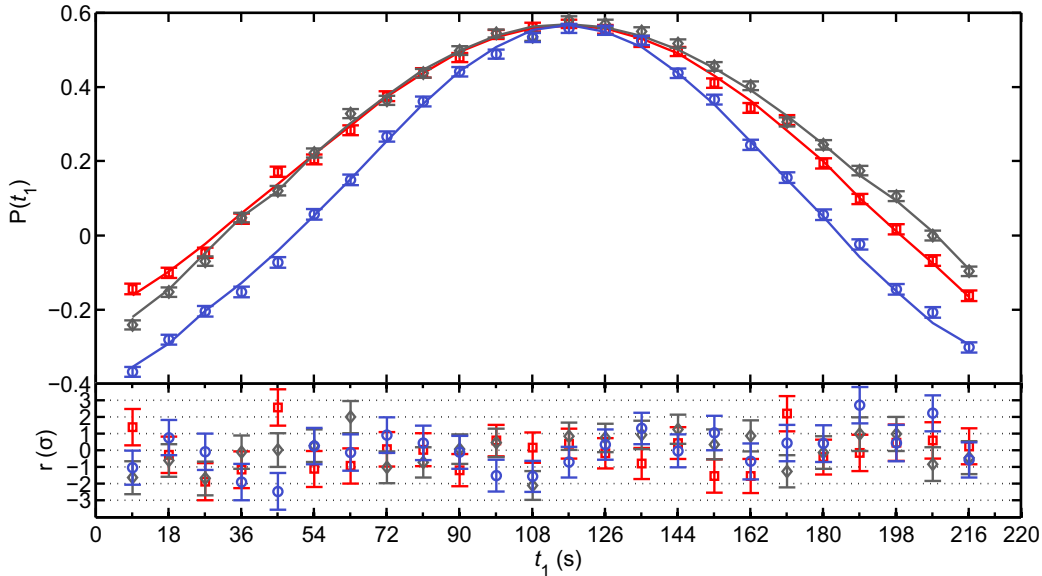


Figure 3: Measured UCN spin-echo signal for three nominal magnetic field gradients. Red squares: $\partial B_z/\partial z = -18$ pT/cm; black diamonds: 10 pT/cm; blue circles: 38 pT/cm. The lines represent the best fit to the data of equation (5), using (7) and (8). The residuals are $r = P(t_1)_{\text{fit}} - P(t_1)_{\text{exp}}$ measured in units of the average uncertainty.

As the observed polarization at $t_1 = T/2$ was the same for all three measurements, we used an averaged common $\Gamma_2(\epsilon)$ for the fit. Figure 4 shows the extracted energy spectrum. The best fit parameters were: $G_z = 5.7(1.1)$ pT/cm, $a = 0.62(2)$, $b = 1_{-0.0}^{+0.8}$ neV $^{1/2}$, $c = 2.5_{-0.0}^{+1.5}$ neV $^{1/2}$, $E_0 = 8.7_{-0.7}^{+3.1}$ neV, and $E_1 = 30.6_{-0.1}^{+2.0}$ neV, with E_2 fixed at 200 neV. The upper and lower confidence intervals were estimated by carrying out random scans of the parameter space ($\sim 5 \times 10^5$ samples with $\chi^2 < \chi^2_{\text{limit}}$) and selecting the largest and smallest parameter values for which

$$\chi^2_{\text{limit}} = \chi^2_{\text{min}} \left(1 + \frac{p}{n-p} F_\alpha(n, n-p) \right), \quad (9)$$

where F_α is the inverse cumulative function of the statistical F -distribution for an $\alpha = 68.3\%$ confidence level with $p = 6$ free parameters and $(n-p) = 66$ degrees of freedom [29]. The values for the lower bounds for $b = 1$ neV $^{1/2}$ and $c = 2.5$ neV $^{1/2}$ were chosen for smooth physical edges while changes in χ^2 for even lower values could be ruled out. The average energy $\langle E \rangle$ of the measured spectrum is $28.7_{-1.4}^{+4.8}$ neV, corresponding to a mean velocity at the base of the containment vessel of $\bar{v} = 234_{-6}^{+19}$ cm/s. The observed intrinsic depolarization time is $T_2 = 506(26)$ s, while the calculated dephasing times are $T_2^* = 450(8)$, $438(10)$, and $281(9)$ s for the measurements at nominal $\partial B_z/\partial z = -18, 10, 38$ pT/cm respectively.

The extracted UCN to mercury center-of-mass offset $h_{\text{off}} = 4.8(3)$ mm (95% C.L. uncertainty: ± 0.4 mm) is larger using this method than the value $2.35(5)$ mm [22] deduced from a measurement of the ratio of the precession frequencies of ^{199}Hg atoms to neutrons, $R = \omega_n/\omega_{\text{Hg}}$, after 180 s of storage (see Ref. [22]). We ascribe this difference to the effect on the measurement of R of gravitationally enhanced depolarization, as discussed in [4], and a softening of the spectrum for longer storage times.

Conclusion

We have demonstrated, using simulations, that the analysis of UCN spin-echo resonance signals in combination with a precise knowledge of the ambient magnetic field provides an excellent method by which to reconstruct the energy spectrum of a confined ensemble of neutrons. The method takes advantage of the relative dephasing of spins arising from a gravitationally induced striation of stored UCN of different energies. Based upon this, measured UCN spin-echo signals have been analyzed. They were taken in a controlled magnetic environment which allowed for long inherent coherence times and permitted a FSP time of 216 s. From these measurements it was possible not only to extract the energy spectrum of stored UCNs but also to determine a common gradient offset with a resolution of 1.1 pT/cm. Using an array of vector magnetometers as described in e.g. Ref. [30] will further improve this technique. Obtaining the optimal resolution will also

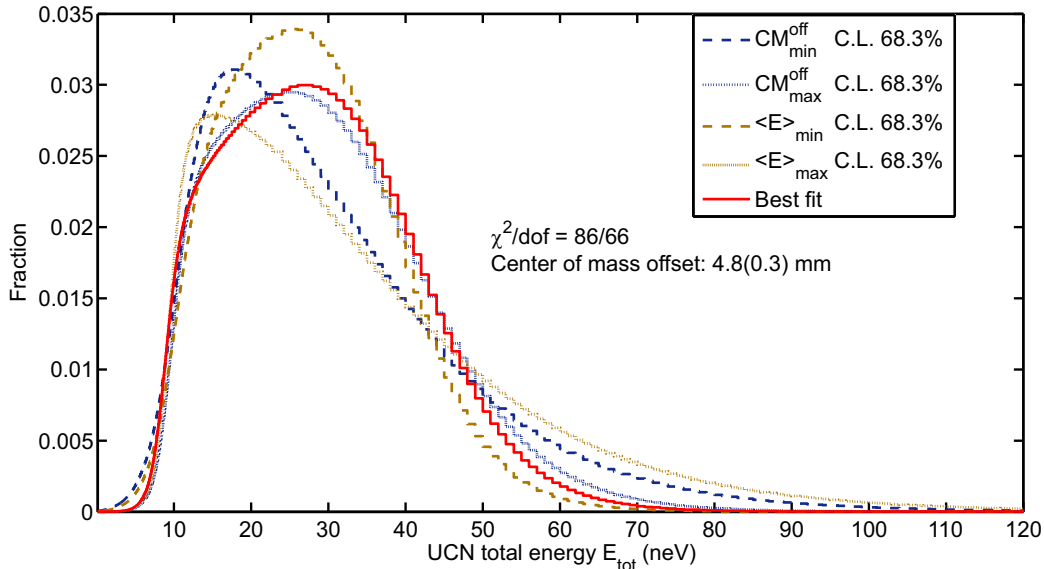


Figure 4: Normalized energy spectra of stored UCNs after 220s storage. The red line indicates the best global fit of equation (5), using (7) and (8), to all three data sets. Further spectra are shown with the highest (lowest) mean energy (brown) and the highest (lowest) center-of-mass offset (blue) within a 68.3% confidence interval.

require an improved understanding of the intrinsic-depolarization processes α , particularly in the limit of very low energies, i.e. $E < H$, including effects of different specularities of wall reflections.

This technique will improve the estimation of energy-spectrum dependent systematic effects in high-precision experiments such as searches for the neutron electric dipole moment [20] and for spin-dependent forces [31]. Alternating measurements with and without the π -pulse at $t_1 = T/2$ could also provide a powerful method to improve the magnetic-field homogeneity of typical UCN spin-precession experiments, such as, for example, neutron EDM searches, where it is known that magnetic field gradients can cause false EDM signals when a co-magnetometer is used [14, 32]. Using the gradient-offset extraction from a spin-echo measurement in combination with a time-resolved gradient measurement by the CsM array may allow one to correct directly for these false-EDM signals in the future.

Acknowledgments

We would like to thank the PSI staff, in particular F. Burri and M. Meier, for their outstanding support. We also gratefully acknowledge the important work carried out by the workshops throughout the collaborating institutes and the computational power provided by the PL-Grid infrastructure. One of us (EW) benefited from a PhD fellowship of the research foundation Flanders (FWO). This research was financed in part by the Fund for Scientific Research, Flanders; grant GO A/2010/10 of KU Leuven; the Swiss National Science Foundation Projects 200020-144473 (PSI), 200021-126562 (PSI), 200020-149211 (ETH) and 200020-140421 (Fribourg); and grants ST/K001329/1, ST/M003426/1 and ST/L006472/1 from the UK's Science and Technology Facilities Council (STFC). The original apparatus was funded by grants from the UK's PPARC (now STFC). The LPC Caen and the LPSC acknowledge the support of the French Agence Nationale de la Recherche (ANR) under reference ANR-09-BLAN-0046. Our Polish partners wish to acknowledge support from the National Science Centre, Poland, under grant no. UMO-2012/04/M/ST2/00556.

* Present address: University of Washington, Seattle, United States of America

† Present address: Max-Planck-Institute of Quantum Optics, Garching, Germany.

‡ Present address: LPSC, Université Grenoble Alpes, CNRS/IN2P3, Grenoble, France

§ Present address: LogrusData, Rilkeplatz 8, Vienna, Austria

¶ Present address: Michigan State University, East-Lansing, USA.

** Corresponding autor: philipp.schmidt-wellenburg@psi.ch

[1] E. L. Hahn. Phys. Rev. **80** (1950) 580-594.

- [2] H. Carr and E. Purcell. *Physical Review* **94** (1954) 630.
- [3] F. Mezei. *Zeitschrift für Physik* **255** (1972) 146.
- [4] P. Harris, J. Pendlebury and N. Devenish. *Phys.Rev.* **D89** (2014) 016011.
- [5] C. A. Baker *et al.* *Phys. Rev. Lett.* **97** (2006) 131801.
- [6] G. Ban *et al.* *Phys. Rev. Lett.* **99** (2007) 161603.
- [7] A. Serebrov *et al.* *Phys. Lett. B* **663** (2008) 181.
- [8] S. K. Lamoreaux and R. Golub. *J. Phys. G* **36** (2009) 104002.
- [9] I. Altarev *et al.* *Nucl. Instr. and Meth. in Phys. Res. A* **611** (2009) 133 .
- [10] I. Altarev *et al.* *EPL* **92** (2010) 51001.
- [11] A. Serebrov *et al.* *JETP Letters* **91** (2010) 6.
- [12] G. Cates, S. Schaefer and W. Happer. *Phys. Rev. A* **37** (1988) 2877.
- [13] D. D. McGregor. *Phys. Rev. A* **41** (1990) 2631.
- [14] J. M. Pendlebury *et al.* *Phys. Rev. A* **70** (2004) 032102.
- [15] R. Schmid, B. Plaster and B. W. Filippone. *Phys. Rev. A* **78** 023401.
- [16] R. Golub, R. Rohm and C. Swank. *Phys. Rev. A* **83** (2011) 023402.
- [17] G. Pignol and S. Rocchia. *Phys. Rev. A* **85** (2012) 042105.
- [18] A. Knecht. Towards a new measurement of the neutron electric dipole moment. Ph.D. thesis, Universität Zürich (2009).
- [19] S. Filipp *et al.* *Phys. Rev. Lett.* **102** (2009) 030404.
- [20] C. Baker *et al.* *Phys. Proc.* **17** (2011) 159.
- [21] J. Pendlebury and D. Richardson. *Nucl. Instr. and Meth. in Phys. Res. A* **337** (1994) 504.
- [22] S. Afach *et al.* *Phys. Lett. B* **739** (2014) 128.
- [23] K. Bodek *et al.* *Phys. Proc.* **17** (2011) 259.
- [24] C. Baker *et al.* *Nucl. Instr. and Meth. in Phys. Res. A* **736** (2014) 184.
- [25] P. Knowles *et al.* *Nucl. Instr. and Meth. in Phys. Res. A* **611** (2009) 306.
- [26] S. Afach *et al.* submitted to *Eur. Phys. J. A* (2015) (arXiv:1502.06876).
- [27] B. Lauss. *Phys. Proc.* **51** (2013) 98.
- [28] K. Green *et al.* *Nucl. Instr. and Meth. in Phys. Res. A* **404** (1998) 381.
- [29] D. Rogers. *Nucl. Instrum. Meth.* **127** (1975) 253.
- [30] S. Afach *et al.* submitted to *Appl. Phys. Lett.* (2015).
- [31] S. Afach *et al.* *Phys. Lett. B* **745** (2015) 58.
- [32] S. Afach *et al.* submitted to *Eur. Phys. J. D* (2015) (arXiv:1503.08651).